Stability of stochastic impulsive reaction-diffusion neural networks with S-type distributed delays and its application to image encryption

Wei, Tengda; Lin, Ping; Wang, Yangfan; Wang, Linshan

Published in:
Neural Networks

DOI:
10.1016/j.neunet.2019.03.016

Publication date:
2019

Wei, T, Lin, P, Wang, Y & Wang, L 2019, 'Stability of stochastic impulsive reaction-diffusion neural networks with S-type distributed delays and its application to image encryption' Neural networks : the official journal of the International Neural Network Society, vol. 116, pp. 35-45. https://doi.org/10.1016/j.neunet.2019.03.016

Stability of stochastic impulsive reaction-diffusion neural networks with S-type distributed delays and its application to image encryption

Tengda Wei[a,b], Ping Lin[b], Yangfan Wang[c,*], Linshan Wang[a,*]

[a] *School of Mathematical Sciences, Ocean University of China, Qingdao 266100, China*
[b] *Department of Mathematics, University of Dundee, Dundee DD1 4HN, Scotland, United Kingdom*
[c] *Ministry of Education Key Laboratory of Marine Genetics and Breeding, College of Marine Life Sciences, Ocean University of China, Qingdao 266003, China*

Abstract

In this paper, we study stochastic impulsive reaction-diffusion neural networks with S-type distributed delays, aiming to obtain the sufficient conditions for global exponential stability. First, an impulsive inequality involving infinite delay is introduced and the asymptotic behaviour of its solution is investigated by the truncation method. Then, global exponential stability in the mean-square sense of the stochastic impulsive reaction-diffusion system is studied by constructing a simple Lyapunov-Krasovskii functional where the S-type distributed delay is handled by the impulsive inequality. Numerical examples are also given to verify the effectiveness of the proposed results. Finally, the obtained theoretical results are successfully applied to an image encryption scheme based on bit-level permutation and the stochastic neural networks.

Keywords: Stochastic reaction-diffusion neural network, Impulse, S-type distributed delay, Image encryption

2010 MSC: 34D06, 90B15, 34A37, 68U10

1. Introduction

In recent years, stochastic neural networks (SNNs) have been intensely investigated due to their wide existence in our daily life. The stochastic perturbation in SNNs

*Corresponding authors.
Email addresses: tdwei123@163.com (Tengda Wei), plin@maths.dundee.ac.uk (Ping Lin), yfwang@ouc.edu.cn) (Yangfan Wang), wangls@ouc.edu.cn (Linshan Wang)

not only distinguishes SNNs from deterministic neural networks, but also brings essential change to the dynamical behaviour of neural networks. Therefore, many researchers have studied the dynamical behaviour of SNNs, such as existence-uniqueness of solutions, periodic oscillatory behaviour, stability properties, and synchronization [1, 2, 11, 19, 21, 26, 34, 47]. In particular, stability analysis is undoubtedly one of the most active parts in these researches of SNNs. Such stability studies focus on the SNNs driven by stochastic noise [31], SNNs with Markovian jump [33, 36, 46], SNNs with impulse [4, 12, 16, 28, 44], etc. Among them, the stability analysis of stochastic impulsive neural networks has been widely investigated because the state of SNNs may change abruptly at certain moment of time and the impulse is effective force to stabilise the system (see [10, 23, 39] and references therein).

The diffusion effect widely exists in biological and artificial neural networks [9]. For instance, the interactions arising from the space-distributed structure of the multilayer cellular neural networks can be seen as diffusion phenomenon [24]. Hence, stochastic impulsive reaction-diffusion neural networks (SIRDNNs) have attracted much attention of researchers [29, 35, 40]. On the other hand, the time delay often occurs in the electronic implementation of analog networks because of the finite speed of signal transmission and amplifier switching. Hence, discrete time delays or distributed time delays are included into neural networks [5, 20, 25, 44, 46]. In [31], an S-type distributed delay in terms of Lebesgue-Stieltjes integration, which includes both of the above delays, was incorporated over an infinitely long duration and had better description of hysteresis phenomenon in networks. Since then, the stability analysis of neural networks with S-type distributed delays has also attracted considerable interest [31, 37]. Recently, there are also some significant works about probabilistic delays and model-dependent time delays [3, 32].

For the application of nonlinear systems including neural networks, image encryption is common interest. In [6], Fridrich suggested that there are two procedures for chaos-based image encryption scheme: permutation and diffusion. Since then, many researchers have focused on chaos-based encryption algorithms based on these two procedures [45, 48]. In [4], Chen et al. presented impulsive synchronization criteria of reaction-diffusion delayed neural networks and applied the theoretical results to a spa-

tiotemporal chaotic cryptosystem. Then, Lakshmanan et al. [14] proposed an image encryption algorithm containing pixel permutation and diffusion based on the chaotic signals generated from inertial neural networks with time-varying delays. More development about the application of delayed neural networks to image encryption refers to [4, 14, 27] and references therein. As mentioned above, SIRDNNs with S-type distributed delays can model real world systems well, and the S-type distributed delays sometimes generate chaotic phenomenon which benefits the encryption process of image encryption [37]. However, there is relatively less work about the stability and application of SIRDNNs with S-type distributed delays because the effect of the delay defined on $(-\infty, t_0]$ is difficult to be eliminated and its non-differentiability blocks the way of constructing Lyapunov-Krasovskii functional with distributed term.

Motivated by the aforementioned discussion, we study SIRDNNs with S-type distributed delays and small impulsive disturbance, aiming to obtain the sufficient conditions for global exponential stability in the mean-square sense. The main contribution of this paper can be summarised as follows: (1) stability and boundedness of an impulsive Halanay-type inequality are investigated by differential inequalities and the construction of several comparison functions where the infinite delay is transformed to finite delay by the truncation method and then the sufficient conditions are obtained by the limitation of an infinitesimal; (2) based on the proposed inequality, the S-type distributed delays are handled by truncation method so that the Lyapunov-Krasovskii functional candidate for the stability of SIRDNNs is a simple one without distributed term; (3) the obtained theoretical results are successfully applied to an image encryption scheme based on bit-level permutation and pixel-level diffusion.

This paper is organized as follows: In Section 2, some notations are presented and asymptotic behaviour of an impulsive system is investigated. Based on the inequality, we study global exponential stability of stochastic impulsive reaction-diffusion neural networks with S-type distributed delays in Section 3. The effectiveness of the results is verified by some illustrative examples in Section 4 and the application to an image encryption scheme in Section 5. Finally, some conclusions are drawn in Section 6.

2. Preliminaries and lemmas

In this paper, unless otherwise specified, the following notations are used. A function $\boldsymbol{\phi} : \mathbb{J} \to \mathbb{R}^n$ is piecewise continuous if $\boldsymbol{\phi}(t)$ has at most a finite number of jump discontinuities and $\boldsymbol{\phi}(t^+) = \boldsymbol{\phi}(t)$ for all points on $\mathbb{J}$ where $\mathbb{J} \subseteq \mathbb{R}$. $PC^b(\mathbb{J}, \mathbb{R}^+)$ represents the family of all piecewise continuous bounded functions from $\mathbb{J}$ to $\mathbb{R}^+$ with norm $\|\phi\|_{PC^b(\mathbb{J},\mathbb{R}^+)} = \sup_{\theta\in\mathbb{J}} |\phi(\theta)|$ and $\phi(t_0^-) = \phi(t_0)$. $PC^b = PC^b((-\infty, t_0], \mathbb{R}^+)$. $(\Omega, \mathcal{F}, P)$ is a complete probability space with filtration $\{\mathcal{F}_t\}_{t\geq t_0}$. A stochastic process $\boldsymbol{u}(t) = \boldsymbol{u}(t, \boldsymbol{x}, w)$ is said to be piecewise continuous if for almost all $w \in \Omega$ and $\boldsymbol{x} \in \mathbb{O}$ function $\boldsymbol{u}(t)$ is piecewise continuous. The impulse sequence on $(t_0, +\infty)$ satisfies $t_0 < t_1 < t_2 < \cdots < t_k < \cdots$ and $\lim\limits_{k\to\infty} t_k = +\infty$. $M^2([t_0, +\infty), \mathbb{R}^{n\times m})$ denotes the family of $n\times m$-matrix-valued-measurable function $\boldsymbol{F}(t)$ with $\int_{t_0}^{+\infty} \|\boldsymbol{F}(s)\|^2_{\mathbb{R}^{n\times m}} ds < \infty$. $(L^2(\mathbb{O}))^n$ and $(H_0^1(\mathbb{O}))^n$ are Hilbert spaces with norms $\|u\| = \|u\|_{(L^2(\mathbb{O}))^n} = (\sum_{i=1}^n \int_{\mathbb{O}} |u_i|^2 dx)^{\frac{1}{2}}$ and $\|u\|_{(H_0^1(\mathbb{O}))^n} = (\sum_{i=1}^n \sum_{j=1}^l \int_{\mathbb{O}} (\frac{\partial u_i}{\partial x_j})^2 dx)^{\frac{1}{2}}$. $\mathbb{C}^b_{\mathcal{F}_{t_0}}$ denotes the family of $\mathcal{F}_{t_0}$-measurable bounded stochastic variables with norm $\|\boldsymbol{\varphi}\|_{\mathbb{C}} \triangleq \|\boldsymbol{\varphi}\|_{\mathbb{C}^b_{\mathcal{F}_{t_0}}} = \sup_{\infty<\theta\leq t_0} \mathcal{E}\|\boldsymbol{\varphi}(\theta)\|$ where $\mathcal{E}$ is the expectation operator. $\|\boldsymbol{A}\|_F \triangleq (\mathrm{tr}(\boldsymbol{A}\boldsymbol{A}^T))^{\frac{1}{2}}$ is the Frobenius norm of $\boldsymbol{A} \in \mathbb{R}^{n\times n}$ and tr is the trace operator. $\mathscr{L}_2^0(\Re, (L^2(\mathbb{O}))^n)$ describes the space of Hilbert-Schmidt operators from $\Re \triangleq Q^{\frac{1}{2}}((L^2(\mathbb{O}))^m)$ into $(L^2(\mathbb{O}))^n$ where Q is a positive definite, self-adjoint, Hilbert-Schmidt operator with a finite trace and $\|\Psi\|_* \triangleq \sqrt{\mathrm{tr}(\Psi Q \Psi^*)}$.

Lemma 1 (Poincaré inequality[30]). *Let $\mathbb{O}$ be an open bounded smooth domain in $\mathbb{R}^l$, then $\|\boldsymbol{u}\| \leq \delta^{-1}\|\boldsymbol{u}\|_{(H_0^1(\mathbb{O}))^n}$, $\boldsymbol{u} \in (H_0^1(\mathbb{O}))^n$, where the constant $\delta > 0$ depends on the size of domain $\mathbb{O}$.*

Lemma 2 ([33]). *Let $\boldsymbol{x} \in \mathbb{R}^n$, $\boldsymbol{y} \in \mathbb{R}^n$ and $\kappa > 0$. Then we have*

$$\boldsymbol{x}^T\boldsymbol{y} + \boldsymbol{y}^T\boldsymbol{x} \leq \kappa\boldsymbol{x}^T\boldsymbol{x} + \kappa^{-1}\boldsymbol{y}^T\boldsymbol{y}.$$

Lemma 3. *$\Phi(t, x, y) \in C(\mathbb{R}^+ \times \mathbb{R} \times \mathbb{R}, \mathbb{R})$ is nondecreasing in y for fixed (t, x), and $I_k(x) : \mathbb{R} \to \mathbb{R}$ is nondecreasing in x, $k \in \mathbb{N}^+$. If $\nu(t)$, $\mu(t)$, $\bar{\nu}(t) = \sup_{-\tau\leq\theta\leq 0} \nu(t+\theta)$, $\bar{\mu}(t) = \sup_{-\tau\leq\theta\leq 0} \mu(t+\theta)$ satisfy the following conditions:*

$$\begin{cases} D^+\nu(t) \leq \Phi(t, \nu(t), \bar{\nu}(t)),\ t \geq t_0,\ t \neq t_k, \\ \nu(t_k) \leq I_k(\nu(t_k^-)),\ k \in \mathbb{N}^+, \end{cases} \tag{1}$$

$$\begin{cases} D^+\mu(t) > \Phi(t, \mu(t), \bar{\mu}(t)),\ t \geq t_0,\ t \neq t_k, \\ \mu(t_k) \geq I_k(\mu(t_k^-)),\ k \in \mathbb{N}^+, \end{cases} \tag{2}$$

where $\nu, \mu \in PC^b$*, then* $\nu(t) \leq \mu(t)$ *for* $t \leq t_0$ *implies* $\nu(t) \leq \mu(t)$ *for* $t \in [t_0, +\infty)$.

Proof. The proof will be given in Appendix A. □

Consider the following impulsive Halanay-type inequality: for any $\epsilon \geq 0$, there exists $\tau \geq 0$ such that

$$\begin{cases} \dfrac{d\nu(t)}{dt} \leq a\nu(t) + b \sup\limits_{-\tau \leq \theta \leq 0} \nu(t+\theta) + o(\epsilon), t \neq t_k, t \geq t_0, \\ \nu(t_k) \leq c_k \nu(t_k^-),\ k \in \mathbb{N}^+, \end{cases} \tag{3}$$

where $b \geq 0$, $o(\epsilon) \geq 0$, $\lim_{\epsilon \to 0} o(\epsilon) = 0$, and $\nu(t) \in PC^b$. Denote $\gamma = \sup_{k \in \mathbb{N}^+}\{c_k\}$ and $\phi(\theta) \triangleq \nu(\theta)$ for $\theta \leq t_0$. If $0 < \gamma \leq 1$, $\gamma = c_k$ and $\rho = t_k - t_{k-1}$ for all $k \in \mathbb{N}^+$. If $\gamma > 1$, $\rho = \inf_{k \in \mathbb{N}^+}\{t_k - t_{k-1}\} > 0$. Then, we shall establish the sufficient conditions for stability of system (3) with small impulsive disturbance $0 < \gamma \leq 1$ and boundedness for large impulsive disturbance $\gamma > 1$.

Lemma 4. *If* $0 < \gamma < 1$, $a + \frac{b}{\gamma} > 0$*, and* $a + \frac{b}{\gamma} + \frac{\ln \gamma}{\rho} < 0$*, then there exist positive constants* M *and* λ *such that* $\nu(t) \leq Me^{-\lambda(t-t_0)}\|\phi\|_{PC^b}$ *for* $t \in [t_0, +\infty)$.

Proof. The proof will be presented in Appendix B. □

Remark 1. When $\gamma = 1$, the impulsive Halanay-type inequality degenerates to an inequality without impulse which has been studied in [37] under the stability condition $a + b < 0$. Therefore, it is straightforward to deduce the following result.

Lemma 5. *If* $0 < \gamma \leq 1$ *and* $a + \frac{b}{\gamma} < 0$*, then there exist positive constants* M *and* λ *such that* $\nu(t) \leq Me^{-\lambda(t-t_0)}\|\phi\|_{PC^b}$ *for* $t \in [t_0, +\infty)$.

Lemma 6. *If* $0 < \gamma < 1$ *and* $a + \frac{b}{\gamma} + \frac{\ln \gamma}{\rho} < 0$*, then there exist positive constants* M *and* λ *such that* $\nu(t) \leq Me^{-\lambda(t-t_0)}\|\phi\|_{PC^b}$ *for* $t \in [t_0, +\infty)$.

Proof. The proof will be given in Appendix C. □

Remark 2. From the considered differential inequality (3) and Lemma 6, we see that the infinite delayed system with certain conditions is transformed to a finite delayed system with an infinitesimal by the truncation method. Therefore, for a class of infinite delayed system, we can impose conditions on the delay term toward stability after the limitation of the infinitesimal. Moreover, the obtained results generalise Halanay inequality [8], inequalities with infinite delay [31, 37], and other impulsive inequalities with finite delay [15, 39, 42] to be suitable for infinite delayed impulsive system.

Lemma 7. *If* $\gamma > 1$ *and* $a + b\gamma + \frac{\ln \gamma}{\rho} < 0$*, then* $\nu(t)$ *in inequality* (3) *is bounded.*

Proof. The proof will be presented in Appendix D. □

Note that we can obtain boundedness of the impulsive system (3) with $\gamma > 1$, but the stability vanishes. In order to explore the reason, we consider a degenerate case of (3) with finite delay:

$$\begin{cases} \dfrac{d\tilde{\nu}(t)}{dt} \leq a\tilde{\nu}(t) + b\tilde{\nu}(t-\tau), t \neq t_k, t \geq t_0, \\ \tilde{\nu}(t_k) \leq c_k \tilde{\nu}(t_k^-),\ k \in \mathbb{N}^+, \end{cases} \tag{4}$$

where $\tau > 0$, $b \geq 0$, $\tilde{\nu}(t) \in PC^b([-\tau, t_0], \mathbb{R}^+)$. Denote $\gamma = \sup_{k \in \mathbb{N}^+} \{c_k\}$ and $\tilde{\phi}(\theta) \triangleq \tilde{\nu}(\theta)$ for $-\tau \leq t \leq t_0$. Inspired from Theorem 1 in [10], we have the following result.

Lemma 8. *If* $\gamma > 1$ *and* $a + b\gamma + \frac{\ln \gamma}{\rho} < 0$*, then there exist positive constants* M *and* λ *such that* $\tilde{\nu}(t) \leq Me^{-\lambda(t-t_0)}\|\phi\|_{PC^b}$ *for* $t \in [t_0, +\infty)$.

Proof. The proof will be given in Appendix E. □

Remark 3. Comparison of Lemma 7 and 8 indicates that the instability of impulsive system (3) with $\gamma > 1$ may originate from infinite delay. To obtain stability, stricter conditions are needed to be imposed on the delay term.

3. Stability analysis of SIRDNNs

First, we consider the following SIRDNNs with S-type distributed delays

$$\begin{cases} d\boldsymbol{u}(t,\boldsymbol{x}) = [\nabla\cdot(\boldsymbol{D}(t,\boldsymbol{x})\circ\nabla\boldsymbol{u}(t,\boldsymbol{x})) + \boldsymbol{A}(t)\boldsymbol{u}(t,\boldsymbol{x}) + \boldsymbol{F}(t,\boldsymbol{u}) \\ \qquad\qquad + \boldsymbol{F}(t,\mathcal{S}(\boldsymbol{u}))]dt + \boldsymbol{G}(t,\mathcal{S}(\boldsymbol{u}))d\boldsymbol{W}(t,\boldsymbol{x}),\ t\geq t_0,\ t\neq t_k, \\ \boldsymbol{u}(t_k,\boldsymbol{x}) = (\boldsymbol{I}+\boldsymbol{C}_k)\boldsymbol{u}(t_k^-,\boldsymbol{x}), \end{cases} \tag{5}$$

with Dirichlet boundary condition and initial condition

$$\boldsymbol{u}(t,\boldsymbol{x})|_{\boldsymbol{x}\in\partial\mathbb{O}} = 0,\ t\geq t_0;\ \boldsymbol{u}(\theta,\boldsymbol{x}) = \boldsymbol{\varphi}(\theta,\boldsymbol{x})\in\mathbb{C}^b_{\mathcal{F}_{t_0}},\ \theta\in(-\infty,t_0],\ \boldsymbol{x}\in\mathbb{O}, \tag{6}$$

where $\boldsymbol{u}(t,\boldsymbol{x}) = (u_1(t,\boldsymbol{x}),\cdots,u_n(t,\boldsymbol{x}))^T$, $\boldsymbol{D}(t,\boldsymbol{x}) = (D_{ij}(t,\boldsymbol{x}))_{n\times l}$, $D_{ij}(t,\boldsymbol{x})\geq\tilde{D}_{ij}>0$, $\nabla\cdot(\boldsymbol{D}(t,\boldsymbol{x})\circ\nabla\boldsymbol{u}) = (\sum_{j=1}^{l}\frac{\partial(D_{1j}(t,\boldsymbol{x})\frac{\partial u_1}{\partial x_j})}{\partial x_j},\cdots,\sum_{j=1}^{l}\frac{\partial(D_{nj}(t,\boldsymbol{x})\frac{\partial u_n}{\partial x_j})}{\partial x_j})^T$, and $\circ$ denotes Hadamard product. Besides, $\boldsymbol{A}(t) = \mathrm{diag}(A_1(t),A_2(t),\cdots,A_n(t))$, $A_i(t)\leq\tilde{A}_i$, $\boldsymbol{F} = (f_1,f_2,\cdots,f_n)^T$, and $\boldsymbol{G} = (G_{ij})_{n\times m}\in\mathbb{M}_2^{n,m}(t_0,t)$ [7]. $\mathcal{S}(\boldsymbol{u}) = \int_{-\infty}^{0}d\boldsymbol{\eta}(\theta)\boldsymbol{u}(t+\theta,\boldsymbol{x})$ is Lebesgue-Stieltjes integrable and $\boldsymbol{\eta}(\theta)$ is non-decreasing bounded variation function which satisfies $\int_{-\infty}^{0}d\boldsymbol{\eta}(\theta) = (\hat{\eta}_{ij})_{n\times n}$ and $\hat{\eta}_{ij}>0$. $\mathbb{O}$ is an open bounded and connected subset of R^l with a sufficient regular boundary $\partial\mathbb{O}$. $\boldsymbol{W}(t,\boldsymbol{x})$ is an infinite dimensional Q-Wiener process [7]. $\boldsymbol{I}$ and $\boldsymbol{C}_k$ are the identical and impulsive matrices. Unless otherwise specified, we assume that

(H1) there exists a positive bounded function $L(t)$ such that $\|\boldsymbol{F}(t,\varsigma_1)-\boldsymbol{F}(t,\varsigma_2)\|\vee\|\boldsymbol{G}(t,\varsigma_1)-\boldsymbol{G}(t,\varsigma_2)\|_*\leq L(t)\|\varsigma_1-\varsigma_2\|$, where $t\in[t_0,+\infty)$, $\varsigma_1,\varsigma_2\in(L^2(\mathbb{O}))^n$.

(H2) $\boldsymbol{F}(t,0)\in M^2([t_0,+\infty),\mathbb{R}^n)$, $\boldsymbol{G}(t,0)\in M^2([t_0,+\infty),\mathbb{R}^{n\times m})$.

According to Theorem 5.1 in [38], system (5) has a unique mild solution for $t\in[t_0,+\infty)$. Then, we shall have the following results for stability of system (5)-(6) with small impulsive disturbance and boundedness for large impulsive disturbance.

Theorem 1. *Assume that H1 and H2 hold. Then system* (5)-(6) *is globally exponentially stable in the mean-square sense, if there exists a positive constant* κ *such that* $0<\gamma<1$,

$$-2\delta^2\min_{ij}\{\tilde{D}_{ij}\}+2\max_{i}\{\tilde{A}_i\}+2\kappa+\kappa^{-1}\tilde{L}^2+2n(1+\kappa^{-1})\|\hat{\boldsymbol{\eta}}\|_F^2\tilde{L}^2/\gamma+\frac{\ln\gamma}{\rho}<0, \tag{7}$$

where $\tilde{L} = \sup_{t\geq t_0}L(t)$, $\gamma = \sup_{k\in\mathbb{N}^+}\|\{\boldsymbol{I}+\boldsymbol{C}_k\|_F^2\}$ *and* $\rho = t_k - t_{k-1}$ *for* $k\in\mathbb{N}^+$.

Proof. Given $\boldsymbol{\varphi} \in \mathbb{C}^b_{\mathcal{F}_{t_0}}$, we write $\boldsymbol{u}(t,\boldsymbol{x}) = \boldsymbol{u}(t,\boldsymbol{x};\boldsymbol{\varphi})$ and define a Lyapunov-Krasovskii functional candidate by $V(t,\boldsymbol{u}(t,\boldsymbol{x})) = \|\boldsymbol{u}(t,\boldsymbol{x})\|^2$. We denote $V(t,\boldsymbol{u}(t,\boldsymbol{x}))$ by $V(t)$. For $t \in (t_{k-1}, t_k)$, $k \in \mathbb{N}^+$, thanks to Itô formula [18], we have

$$dV(t) = \mathcal{L}V dt + 2\int_{\mathbb{O}} \boldsymbol{u}^T \boldsymbol{G} d\boldsymbol{W} d\boldsymbol{x}, \tag{8}$$

where

$$\begin{aligned}
\mathcal{L}V = &\int_{\mathbb{O}} \boldsymbol{u}^T(t,\boldsymbol{x})(\nabla\cdot(\boldsymbol{D}(t,\boldsymbol{x})\circ\nabla\boldsymbol{u}(t,\boldsymbol{x})))d\boldsymbol{x} \\
&+ \int_{\mathbb{O}} (\nabla\cdot(\boldsymbol{D}(t,\boldsymbol{x})\circ\nabla\boldsymbol{u}(t,\boldsymbol{x})))^T\boldsymbol{u}(t,\boldsymbol{x})]d\boldsymbol{x} \\
&+ \int_{\mathbb{O}} [\boldsymbol{u}^T(t,\boldsymbol{x})\boldsymbol{A}(t)\boldsymbol{u}(t,\boldsymbol{x}) + \boldsymbol{u}(t,\boldsymbol{x})^T\boldsymbol{A}^T(t)\boldsymbol{u}(t,\boldsymbol{x})]d\boldsymbol{x} \\
&+ \int_{\mathbb{O}} [\boldsymbol{u}^T(t,\boldsymbol{x})\boldsymbol{F}(t,\boldsymbol{u}) + \boldsymbol{F}^T(t,\boldsymbol{u})\boldsymbol{u}(t,\boldsymbol{x})]d\boldsymbol{x} \\
&+ \int_{\mathbb{O}} [\boldsymbol{u}^T(t,\boldsymbol{x})\boldsymbol{F}(t,\mathcal{S}(\boldsymbol{u})) + \boldsymbol{F}^T(t,\mathcal{S}(\boldsymbol{u}))\boldsymbol{u}(t,\boldsymbol{x})]d\boldsymbol{x} \\
&+ \text{tr}(\boldsymbol{G}Q\boldsymbol{G}^*) \triangleq \sum_{i=1}^{6}\mathcal{L}V_i.
\end{aligned} \tag{9}$$

Taking expectation of $dV(t)$, we know that $\frac{d\mathcal{E}V(t)}{dt} = \mathcal{E}\mathcal{L}V$. From Gauss formula, Dirichlet boundary condition and Poincaré inequality, we have

$$\sum_{j=1}^{l}\int_{\mathbb{O}} u_i(t,\boldsymbol{x})\frac{\partial}{\partial x_j}(D_{ij}(t,\boldsymbol{x})\frac{\partial u_i(t,\boldsymbol{x})}{\partial x_j})d\boldsymbol{x} \le -\sum_{j=1}^{l}\int_{\mathbb{O}} D_{ij}(t,\boldsymbol{x})(\frac{\partial u_i(t,\boldsymbol{x})}{\partial x_j})^2 d\boldsymbol{x}, \tag{10}$$

indicating that, $\mathcal{E}\mathcal{L}V_1 + \mathcal{E}\mathcal{L}V_2 \le -2\delta^2 \min_{ij}\{\tilde{D}_{ij}\}\mathcal{E}V(t)$. Obviously, $\mathcal{E}\mathcal{L}V_3 \le 2\max_i \{A_i(t)\}\mathcal{E}V(t)$. From Lemma 2 and (H1), we obtain

$$\begin{aligned}
\mathcal{E}\mathcal{L}V_4 &\le \kappa\mathcal{E}\int_{\mathbb{O}} \boldsymbol{u}^T(t,\boldsymbol{x})\boldsymbol{u}(t,\boldsymbol{x})d\boldsymbol{x} + \kappa^{-1}\mathcal{E}\int_{\mathbb{O}} \boldsymbol{F}^T(t,\boldsymbol{u})\boldsymbol{F}(t,\boldsymbol{u})d\boldsymbol{x}, \\
&\le \kappa\mathcal{E}V(t) + \kappa^{-1}L^2(t)\mathcal{E}\int_{\mathbb{O}} \boldsymbol{u}^T(t,\boldsymbol{x})\boldsymbol{u}(t,\boldsymbol{x})d\boldsymbol{x} \le (\kappa + \kappa^{-1}L^2(t))\mathcal{E}V(t),
\end{aligned} \tag{11}$$

$$\begin{aligned}
\mathcal{E}\mathcal{L}V_5 &\le \kappa\mathcal{E}\int_{\mathbb{O}} \boldsymbol{u}^T(t,\boldsymbol{x})\boldsymbol{u}(t,\boldsymbol{x})d\boldsymbol{x} + \kappa^{-1}\mathcal{E}\int_{\mathbb{O}} \boldsymbol{F}^T(t,\mathcal{S}(\boldsymbol{u}))\boldsymbol{F}(t,\mathcal{S}(\boldsymbol{u}))d\boldsymbol{x} \\
&\le \kappa\mathcal{E}V(t) + \kappa^{-1}L^2(t)\mathcal{E}\|\int_{-\infty}^{0} d\boldsymbol{\eta}(\theta)\boldsymbol{u}(t+\theta,\boldsymbol{x})\|^2.
\end{aligned} \tag{12}$$

Since $\int_{-\infty}^{0} d\eta_{ij}(\theta) = \hat{\eta}_{ij} > 0$ $(i,j = 1,2,\cdots,n)$ and $\eta_{ij}(\theta)$ is non-decreasing bounded variation function, there exists a constant $\tau \geq t$ such that $\int_{-\infty}^{-\tau} d\eta_{ij}(\theta) \leq \epsilon$ for any $\epsilon \geq 0$ and $i,j = 1,2,\cdots,n$. Therefore,

$$\begin{aligned}
&\mathcal{E}\| \int_{-\infty}^{0} d\boldsymbol{\eta}(\theta)\boldsymbol{u}(t+\theta,\boldsymbol{x})\|^2 \\
&\leq 2\mathcal{E}\| \int_{-\tau}^{0} d\boldsymbol{\eta}(\theta)\boldsymbol{u}(t+\theta,\boldsymbol{x})\|^2 + 2\mathcal{E}\| \int_{-\infty}^{-\tau} d\boldsymbol{\eta}(\theta)\boldsymbol{u}(t+\theta,\boldsymbol{x})\|^2 \\
&\leq 2n\|\hat{\boldsymbol{\eta}}\|_F^2 \sup_{-\tau\leq\theta\leq 0} \mathcal{E}\|\boldsymbol{u}(t+\theta,\boldsymbol{x})\|^2 + 2n\epsilon^2\mathcal{E}\|\boldsymbol{\varphi}\|_{\mathbb{C}}^2,
\end{aligned} \tag{13}$$

and

$$\mathcal{E}\mathcal{L}V_5 \leq \kappa\mathcal{E}V(t) + 2n\kappa^{-1}\|\hat{\boldsymbol{\eta}}\|_F^2 L(t)^2 \sup_{-\tau\leq\theta\leq 0} \mathcal{E}V(t+\theta) + 2n\epsilon^2\kappa^{-1}L(t)^2\mathcal{E}\|\boldsymbol{\varphi}\|_{\mathbb{C}}^2. \tag{14}$$

Besides, from (H1), we see that

$$\begin{aligned}
\mathcal{E}\mathcal{L}V_6 &\leq L(t)^2\mathcal{E}\| \int_{-\infty}^{0} d\boldsymbol{\eta}(\theta)\boldsymbol{u}(t+\theta,\boldsymbol{x})\|^2 \\
&\leq 2n\|\hat{\boldsymbol{\eta}}\|_F^2 L(t)^2 \sup_{-\tau\leq\theta\leq 0} \mathcal{E}V(t+\theta) + 2n\epsilon^2 L(t)^2\mathcal{E}\|\boldsymbol{\varphi}\|_{\mathbb{C}}^2.
\end{aligned} \tag{15}$$

Thus, combining (8)-(15), we have

$$\begin{aligned}
\frac{d\mathcal{E}V(t)}{dt} &\leq a(t)\mathcal{E}V(t) + b(t) \sup_{-\tau\leq\theta\leq 0} \mathcal{E}V(t+\theta) + d(t)\epsilon^2, \\
&\leq \tilde{a}\mathcal{E}V(t) + \tilde{b} \sup_{-\tau\leq\theta\leq 0} \mathcal{E}V(t+\theta) + \tilde{d}\epsilon^2,
\end{aligned} \tag{16}$$

where $a(t) = -2\delta^2 \min_{ij}\{\tilde{D}_{ij}\} + 2\max_{i}\{A_i(t)\} + 2\kappa + \kappa^{-1}L^2(t)$, $b(t) = 2n(1+\kappa^{-1})\|\hat{\boldsymbol{\eta}}\|_F^2 L^2(t)$, $d(t) = 2n(1+\kappa^{-1})L^2(t)\mathcal{E}\|\boldsymbol{\varphi}\|_{\mathbb{C}}^2$, $\tilde{a} = -2\delta^2 \min_{ij}\{\tilde{D}_{ij}\} + 2\max_{i}\{\tilde{A}_i\} + 2\kappa + \kappa^{-1}\tilde{L}^2$, $\tilde{b} = 2n(1+\kappa^{-1})\|\hat{\boldsymbol{\eta}}\|_F^2\tilde{L}^2$, and $\tilde{d} = 2n(1+\kappa^{-1})\tilde{L}^2\mathcal{E}\|\boldsymbol{\varphi}\|_{\mathbb{C}}^2$. When $t = t_k$, $\mathcal{E}V(t_k) \leq \gamma\mathcal{E}V(t_k^-)$ where $\gamma = \sup_{k\in\mathbb{N}^+}\{\|\boldsymbol{I} + \boldsymbol{C}_k\|_F^2\}$. When $t \leq t_0$, $\mathcal{E}V(t) = \mathcal{E}\|\boldsymbol{\varphi}(t)\|^2 \in PC^b$. From Lemma 6 and (7), we see that there exist positive constants M and λ such that $\mathcal{E}\|\boldsymbol{u}(t,\boldsymbol{x})\|^2 \leq Me^{-\lambda(t-t_0)}\mathcal{E}\|\boldsymbol{\varphi}\|_{\mathbb{C}}^2$. Then, system (5)-(6) is globally exponentially stable in the mean-square sense. □

Corollary 1. Assume that H1 and H2 hold. Then system (5)-(6) is globally exponentially stable in the mean-square sense, if $0 < \gamma < 1$,

$$-2\delta^2 \min_{ij}\{\tilde{D}_{ij}\} + 2\max_{i}\{\tilde{A}_i\} + 2 + \tilde{L}^2 + 4n\|\hat{\boldsymbol{\eta}}\|_F^2\tilde{L}^2/\gamma + \frac{\ln\gamma}{\rho} < 0, \tag{17}$$

where $\tilde{L} = \sup_{t\geq t_0} L(t)$, $\gamma = \|\boldsymbol{I} + \boldsymbol{C}_k\|_F^2$ and $\rho = t_k - t_{k-1}$ for all $k \in \mathbb{N}^+$.

Remark 4. It is noted from (7) that impulsive coefficient can be treated as a positive factor of stability if the impulsive interval and γ are small enough, which indicates the potential of impulsive control for SRDNNs.

Theorem 2. *Assume that H1 and H2 hold. Then system* (5)-(6) *is bounded in the mean-square sense, if there exists a positive constant* κ *such that* $\gamma > 1$*,*

$$-2\delta^2 \min_{ij}\{\tilde{D}_{ij}\}+2\max_{i}\{\tilde{A}_i\}+2\kappa+\kappa^{-1}\tilde{L}^2+2n\gamma(1+\kappa^{-1})\|\hat{\boldsymbol{\eta}}\|_F^2\tilde{L}^2+\frac{\ln\gamma}{\rho} < 0, \quad (18)$$

where $\tilde{L} = \sup_{t\geq t_0} L(t)$, $\gamma = \sup_{k\in\mathbb{N}^+}\{\|\boldsymbol{I} + \boldsymbol{C}_k\|_F^2\}$ *and* $\rho = \inf_{k\in\mathbb{N}^+}\{t_k - t_{k-1}\} > 0$.

Remark 5. For SIRDNNs with finite delays, global exponential stability can be easily obtained by Lemma 6 and 8 when $\gamma > 0$, which indicates that the reason why global stability vanishes for $\gamma > 1$ lies in S-type distributed delays.

Next, we consider impulsive control of the following stochastic reaction-diffusion neural networks

$$\begin{cases} d\bar{\boldsymbol{u}}(t,\boldsymbol{x}) = [\nabla\cdot(\boldsymbol{D}(t,\boldsymbol{x})\circ\nabla\bar{\boldsymbol{u}}(t,\boldsymbol{x})) + \boldsymbol{A}(t)\bar{\boldsymbol{u}}(t,\boldsymbol{x}) + \boldsymbol{B}_1(t)\bar{\boldsymbol{F}}_1(\bar{\boldsymbol{u}}) \\ \qquad\qquad + \boldsymbol{B}_2(t)\bar{\boldsymbol{F}}_2(\mathcal{S}(\bar{\boldsymbol{u}}))]dt + \boldsymbol{E}(t)\bar{\boldsymbol{G}}(\mathcal{S}(\bar{\boldsymbol{u}}))d\boldsymbol{W}(t,\boldsymbol{x}),\ t\geq t_0,\ t\neq t_k \\ \bar{\boldsymbol{u}}(t_k,\boldsymbol{x}) = \boldsymbol{C}_k\bar{\boldsymbol{u}}(t_k^-,\boldsymbol{x}), \\ \bar{\boldsymbol{u}}(\theta,\boldsymbol{x}) = \bar{\boldsymbol{\varphi}}(\theta,\boldsymbol{x}) \in \mathbb{C}^b_{\mathcal{F}_{t_0}},\ \theta\in(-\infty,t_0],\ \boldsymbol{x}\in\mathbb{O}, \end{cases} \quad (19)$$

with the homogeneous Dirichlet boundary condition, where $\boldsymbol{B}_1(t) = (B_{1ij}(t))_{n\times n}$, $\boldsymbol{B}_2(t) = (B_{2ij}(t))_{n\times n}$, $\boldsymbol{E}(t) = (E_{ij}(t))_{n\times n}$, and $\boldsymbol{C}$ is the impulsive controller gain to be determined and $\rho = t_k - t_{k-1}$ for all $k \in \mathbb{N}^+$. Assume that the following conditions hold,

(H3) $\|\bar{\boldsymbol{F}}_1(\varsigma_1) - \bar{\boldsymbol{F}}_1(\varsigma_2)\| \vee \|\bar{\boldsymbol{F}}_2(\varsigma_1) - \bar{\boldsymbol{F}}_2(\varsigma_2)\| \vee \|\bar{\boldsymbol{G}}(\varsigma_1) - \bar{\boldsymbol{G}}(\varsigma_2)\|_* \leq \bar{L}\|\varsigma_1 - \varsigma_2\|$,

(H4) $D_{ij}(t,\boldsymbol{x}) \geq \bar{D}_{ij} > 0$, $A_i(t) \leq \bar{A}_i$, $|B_{1ij}(t)| \leq \bar{B}_{1ij}$, $|B_{2ij}(t)| \leq \bar{B}_{2ij}$, $|E_{ij}(t)| \leq \bar{E}_{ij}$, where $t \in [t_0,+\infty)$, $i,j = 1,\cdots,n$, and $\varsigma_1,\varsigma_2 \in (L^2(\mathbb{O}))^n$.

Theorem 3. *Assume that H3 and H4 hold. Then the global exponential stability in the mean-square sense of system* (19) *is guaranteed under the impulsive controller*

$\gamma = \sup_{k\in\mathbb{N}^+}\{\|\boldsymbol{C}\|\}_F^2 \in (0,1)$*, if there exists a positive constant* κ *such that*

$$\begin{aligned} -2\delta^2 \min_{ij}\{\bar{D}_{ij}\} + 2\max_{i}\{\bar{A}_i\} + \kappa(\|\bar{\boldsymbol{B}}_1\|_F^2 + \|\bar{\boldsymbol{B}}_2\|_F^2) \\ + \kappa^{-1}\bar{L}^2 + 2n\bar{L}^2\|\hat{\boldsymbol{\eta}}\|_F^2(\kappa^{-1} + \|\bar{\boldsymbol{E}}\|_F^2)/\gamma + \frac{\ln\gamma}{\rho} < 0. \end{aligned} \tag{20}$$

Proof. The details of the proof are similar to those of Theorem 1, so we just give an outline of the proof. Given $\bar{\boldsymbol{\varphi}} \in \mathbb{C}^b_{\mathcal{F}_{t_0}}$, we define a Lyapunov-Krasovskii functional candidate by $\bar{V}(t) = \bar{V}(t, \bar{\boldsymbol{u}}(t,\boldsymbol{x})) = \|\bar{\boldsymbol{u}}(t,\boldsymbol{x})\|^2$. For $t \in (t_{k-1}, t_k)$, $k \in \mathbb{N}^+$, thanks to Itô formula [18], we have

$$d\bar{V}(t) = \mathcal{L}\bar{V}dt + 2\int_{\mathbb{O}} \bar{\boldsymbol{u}}^T \boldsymbol{E}(t)\bar{\boldsymbol{G}}d\boldsymbol{W}d\boldsymbol{x}, \tag{21}$$

where

$$\begin{aligned} \mathcal{L}\bar{V} = &\int_{\mathbb{O}} \bar{\boldsymbol{u}}^T(t,\boldsymbol{x})(\nabla\cdot(\boldsymbol{D}(t,\boldsymbol{x})\circ\nabla\bar{\boldsymbol{u}}(t,\boldsymbol{x})))d\boldsymbol{x} \\ &+ \int_{\mathbb{O}} (\nabla\cdot(\boldsymbol{D}(t,\boldsymbol{x})\circ\nabla\bar{\boldsymbol{u}}(t,\boldsymbol{x})))^T\bar{\boldsymbol{u}}(t,\boldsymbol{x})]d\boldsymbol{x} \\ &+ \int_{\mathbb{O}} [\bar{\boldsymbol{u}}^T(t,\boldsymbol{x})\boldsymbol{A}(t)\bar{\boldsymbol{u}}(t,\boldsymbol{x}) + \bar{\boldsymbol{u}}(t,\boldsymbol{x})^T\boldsymbol{A}^T(t)\bar{\boldsymbol{u}}(t,\boldsymbol{x})]d\boldsymbol{x} \\ &+ \int_{\mathbb{O}} [\bar{\boldsymbol{u}}^T(t,\boldsymbol{x})\boldsymbol{B}_1(t)\bar{\boldsymbol{F}}_1(\bar{\boldsymbol{u}}) + (\boldsymbol{B}_1(t)\bar{\boldsymbol{F}}_1(\bar{\boldsymbol{u}}))^T\bar{\boldsymbol{u}}(t,\boldsymbol{x})]d\boldsymbol{x} \\ &+ \int_{\mathbb{O}} \bar{\boldsymbol{u}}^T(t,\boldsymbol{x})\boldsymbol{B}_2(t)\bar{\boldsymbol{F}}_2(t,\mathcal{S}(\bar{\boldsymbol{u}}))d\boldsymbol{x} + \int_{\mathbb{O}} (\boldsymbol{B}_2(t)\bar{\boldsymbol{F}}_2(t,\mathcal{S}(\bar{\boldsymbol{u}})))^T\bar{\boldsymbol{u}}(t,\boldsymbol{x})d\boldsymbol{x} \\ &+ \mathrm{tr}((\boldsymbol{E}(t)\bar{\boldsymbol{G}})Q(\boldsymbol{E}(t)\bar{\boldsymbol{G}})^*) \triangleq \sum_{i=1}^{6}\mathcal{L}\bar{V}_i. \end{aligned} \tag{22}$$

From Lemma 2, (H3) and (H4), we obtain

$$\begin{aligned} \mathcal{E}\mathcal{L}\bar{V}_4 &\le \kappa\mathcal{E}\int_{\mathbb{O}} \bar{\boldsymbol{u}}^T(t,\boldsymbol{x})\boldsymbol{B}_1(t)\boldsymbol{B}_1^T(t)\bar{\boldsymbol{u}}(t,\boldsymbol{x})d\boldsymbol{x} + \kappa^{-1}\mathcal{E}\int_{\mathbb{O}} \bar{\boldsymbol{F}}_1^T(\bar{\boldsymbol{u}})\bar{\boldsymbol{F}}_1(\bar{\boldsymbol{u}})d\boldsymbol{x}, \\ &\le \kappa\|\boldsymbol{B}_1(t)\|_F^2\mathcal{E}\bar{V}(t) + \kappa^{-1}\bar{L}^2\mathcal{E}\int_{\mathbb{O}} \bar{\boldsymbol{u}}^T(t,\boldsymbol{x})\bar{\boldsymbol{u}}(t,\boldsymbol{x})d\boldsymbol{x} \\ &\le (\kappa\|\bar{\boldsymbol{B}}_1\|_F^2 + \kappa^{-1}\bar{L}^2)\mathcal{E}\bar{V}(t), \end{aligned} \tag{23}$$

$$\begin{aligned} \mathcal{E}\mathcal{L}\bar{V}_5 &\le \kappa\mathcal{E}\int_{\mathbb{O}} \bar{\boldsymbol{u}}^T(t,\boldsymbol{x})\boldsymbol{B}_2(t)\boldsymbol{B}_2^T(t)\bar{\boldsymbol{u}}(t,\boldsymbol{x})d\boldsymbol{x} + \kappa^{-1}\mathcal{E}\int_{\mathbb{O}} \bar{\boldsymbol{F}}_2^T(\mathcal{S}(\bar{\boldsymbol{u}}))\bar{\boldsymbol{F}}_2(\mathcal{S}(\bar{\boldsymbol{u}}))d\boldsymbol{x} \\ &\le \kappa\|\bar{\boldsymbol{B}}_2\|_F^2\mathcal{E}\bar{V}(t) + 2n\kappa^{-1}\bar{L}^2(\|\hat{\boldsymbol{\eta}}\|_F^2 \sup_{-\tau\le\theta\le 0}\mathcal{E}\bar{V}(t+\theta) + \epsilon^2\mathcal{E}\|\bar{\boldsymbol{\varphi}}\|_{\mathbb{C}}^2), \end{aligned} \tag{24}$$

and

$$\begin{aligned}\mathcal{E}\mathcal{L}\bar{V}_7 &\leq \bar{L}^2\|\boldsymbol{E}(t)\|_F^2\mathcal{E}\|\int_{-\infty}^{0} d\boldsymbol{\eta}(\theta)\bar{\boldsymbol{u}}(t+\theta,\boldsymbol{x})\|^2 \\ &\leq 2n\bar{L}^2\|\bar{\boldsymbol{E}}\|_F^2(\|\hat{\boldsymbol{\eta}}\|_F^2 \sup_{-\tau\leq\theta\leq 0}\mathcal{E}\bar{V}(t+\theta)+\epsilon^2\mathcal{E}\|\bar{\boldsymbol{\varphi}}\|_{\mathbb{C}}^2).\end{aligned} \tag{25}$$

Thus, combining (10), (21)-(25), we have

$$\frac{d\mathcal{E}\bar{V}(t)}{dt} \leq \bar{a}\mathcal{E}\bar{V}(t)+\bar{b}\sup_{-\tau\leq\theta\leq 0}\mathcal{E}\bar{V}(t+\theta)+\bar{d}\epsilon^2, \tag{26}$$

where $\bar{a} = -2\delta^2\min_{ij}\{\bar{D}_{ij}\} + 2\max_{i}\{\bar{A}_i\} + \kappa\|\bar{\boldsymbol{B}}_1\|_F^2 + \kappa\|\bar{\boldsymbol{B}}_2\|_F^2 + \kappa^{-1}\bar{L}^2$, $\bar{b} = 2n\bar{L}^2\|\hat{\boldsymbol{\eta}}\|_F^2(\kappa^{-1}+\|\bar{\boldsymbol{E}}\|_F^2)$, and $\bar{d} = 2n\bar{L}^2(\kappa^{-1}+\|\bar{\boldsymbol{E}}\|_F^2)\mathcal{E}\|\bar{\boldsymbol{\varphi}}\|_{\mathbb{C}}^2$. When $t = t_k$, $\mathcal{E}\bar{V}(t_k) \leq \gamma\mathcal{E}\bar{V}(t_k^-)$ where $\gamma = \sup_{k\in\mathbb{N}^+}\{\|\boldsymbol{C}\|_F^2\}$. When $t \leq t_0$, $\mathcal{E}\bar{V}(t) = \mathcal{E}\|\bar{\boldsymbol{\varphi}}(t)\|^2 \in PC^b$. From Lemma 6, we see that system (19) is globally exponentially stable in the mean-square sense, if $0 < \gamma < 1$ and (20) hold. □

Remark 6. In this paper, we establish the stability conditions of SIRDNNs with S-type distributed delays while Refs. [35, 40] does not consider the distributed delays. In most recent works about distributed delays [4, 46, 47], a Lyapunov-Krasovskii functional with distributed term is introduced, however, the suitable Lyapunov-Krasovskii functional with distributed term is usually difficult to find. Here, as the infinite delays are handled by truncation method and an impulsive inequality, we are able to construct a simple Lyapunov-Krasovskii functional candidate without the distributed term. Therefore, the method we used is more effective and general. Besides, we also extend some works about non-autonomous neural networks [13, 22, 43] to impulsive ones.

4. Numerical examples

In this section, two numerical examples are given to illustrate the effectiveness of the obtained results.

Example 1. Consider the following SIRDNN

$$\begin{cases} du(t,x) = [D(t)\Delta u(t,x) - A(t)u(t,x) + f(t,\mathcal{S}(u))]dt \\ \qquad\qquad + g(t,\mathcal{S}(u))dw(t),\ t \neq t_k,\ t \geq 0, \\ u(t_k,x) = (1+C)u(t_k^-,x),\ t_k = k,\ k \in \mathbb{N}^+, \end{cases} \tag{27}$$

with the homogeneous Dirichlet boundary condition, where $x \in [-5,5]$, $D(t) = 0.11 + 0.1\sin(t)$, $A(t) = -5.9 - 0.1\sin^2(t)$, $f(t,\mathcal{S}(u)) = \sin^2(2t)\tanh(\mathcal{S}(u))$, $g(t,\mathcal{S}(u)) = \tanh(\mathcal{S}(u))$, $\eta(\theta) = e^{\theta}$, $\theta \in (-\infty, 0]$, and $C = e^{-1} - 1$. The initial condition is chosen as $\varphi(\theta, x) = \sin(\frac{x}{5})$ for $\theta \in [-100, 0]$ and $\varphi(\theta, x) = 0$ for $\theta \in (-\infty, -100)$. It is easy to check that $0 < \gamma < 1$ and condition (7) holds with $\kappa = \sqrt{\frac{2e+1}{2}}$. Thus, system (27) is globally exponentially stable as shown in Figure 1.

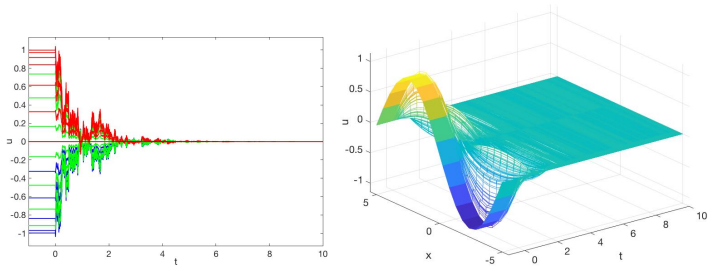

Figure 1: Trajectory simulation of SIRDNN (27) in Example 1.

Example 2. Consider the following stochastic impulsive neural networks

$$\begin{cases} du(t) = [-3.5u(t) + 0.2f(u) + 0.2f(\mathcal{S}(u))]dt \\ \qquad\qquad + 0.2g(\mathcal{S}(u))dw(t),\ t \neq t_k,\ t \geq 0, \\ u(t_k) = 2u(t_k^-),\ t_k = 0.25k,\ k \in \mathbb{N}^+, \end{cases} \tag{28}$$

with the homogeneous Dirichlet boundary condition, where $f(u) = g(u) = \frac{|u+1|+|u-1|}{2}$, $\mathcal{S}(u) = \int_{-\infty}^{0} \eta(\theta)u(t+\theta)d\theta$, and $w(t)$ is the standard Brownian motion. The initial condition is taken as

$$u(\theta) = \begin{cases} M & -1 \leq \theta \leq 0, \\ 0 & \theta < 1. \end{cases}$$

It is easy to check that $\gamma > 1$ and condition (18) holds with $\kappa = \frac{\sqrt{2}}{2}$. Here, we consider two types of delays: distributed delay $\int_{-\infty}^{0} \eta(\theta)u(t+\theta)d\theta = \int_{-\infty}^{0} e^{\theta}u(t+\theta)d\theta$ and discrete delay $\int_{-\infty}^{0} \eta(\theta)u(t+\theta)d\theta = e^{-1}u(t-1)$. From Theorem 2 and Remark 5, system (28) with distributed delay is bounded while the discrete delayed one is globally exponentially stable. Figure 2 illustrates simulation of dynamical behaviour of system (28) with initial conditions $M = 5$ and $M = -5$, which shows the boundedness of the

infinite delayed system and stability of the finite delayed system, in agreement with the theory.

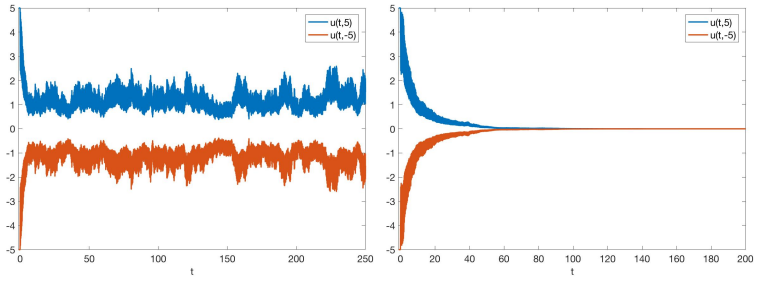

Figure 2: Simulation of system (28) with distributed delay (left) and discrete delay (right) in Example 2.

5. Application to image encryption

In this section, we apply the aforementioned stability analysis to a 2-D drive-response system. Then, the generated drive and response signals are delivered into an image cryptosystem which is built based on bit-level permutation and and pixel-level diffusion inspired by [4, 45, 48].

5.1. Drive-response system

The drive-response system used for image encryption is given by

$$d\boldsymbol{s}(t,x) = [-\boldsymbol{A}\boldsymbol{s}(t,x) + \boldsymbol{B}_1 f(\boldsymbol{s}(t,x)) + \boldsymbol{B}_2 f(\mathcal{S}(\boldsymbol{s}))]dt + \boldsymbol{E}\mathcal{S}(\boldsymbol{s})dw(t), \tag{29}$$

with the homogeneous Dirichlet boundary condition, where $\mathbb{O} = [-10, 10]$, $\boldsymbol{s}(t,x) = (s_1(t,x), s_2(t,x))^T$ is the drive signal (or response signal), $w(t)$ is the standard Brownian motion, $f(\boldsymbol{s}) = \tanh(\boldsymbol{s})$, $\mathcal{S}(\boldsymbol{s}) = \boldsymbol{s}(t-\tau(t),x)$, $\tau(t) = e^t/(1+e^t)$, $\boldsymbol{A} = \boldsymbol{I}$, $\boldsymbol{E} = 1.293\boldsymbol{I}$, and

$$\boldsymbol{B}_1 = \begin{bmatrix} 1.1 & -0.1 \\ -0.5 & 0.45 \end{bmatrix}, \ \boldsymbol{B}_2 = \begin{bmatrix} -1.1 & -0.1 \\ -0.2 & -0.4 \end{bmatrix}.$$

The drive signal $\boldsymbol{s}(t,x)$ and response signal $\tilde{\boldsymbol{s}}(t,x)$ are generated by the following initial conditions

$$s_1(\theta,x)=\sin^2(\frac{x\pi}{2}),\ s_2(\theta,x)=\cos^2(\frac{x\pi}{2}),\ x\in\mathbb{O}\setminus\partial\mathbb{O},$$

$$\tilde{s}_1(\theta,x)=\begin{cases}1,\ x\in\mathbb{O}_k\setminus\partial\mathbb{O};\\ 0,\ \text{otherwise},\end{cases}\quad \tilde{s}_2(\theta,x)=\begin{cases}-1,\ x\in C_{\mathbb{O}}\mathbb{O}_k\setminus\partial\mathbb{O};\\ 0,\ \text{otherwise},\end{cases}$$

where $-1\le\theta\le 0$ and $\mathbb{O}_k=[-10+0.2k,-9.9+0.2k]$ $(k=0,1,\cdots,99)$. From Theorem 1 and 3, it is straightforward to assert that the error signal, defined by $\boldsymbol{e}(t,x)=\boldsymbol{s}(t,x)-\tilde{\boldsymbol{s}}(t,x)$, is globally exponentially stable in the mean-square sense by the impulsive controller $\boldsymbol{e}(t_k,x)=0.22\boldsymbol{e}(t_k^-,x)$ $(t_k=0.14k,\ k\in\mathbb{N}^+)$, that is the synchronization of drive-response signals. As shown in Figure 3, the uncontrolled error signal is unstable and the controlled appears to decay to zero, in agreement with the theory.

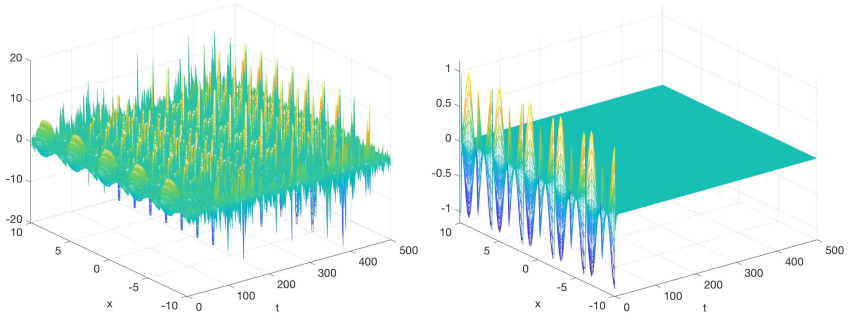

Figure 3: The trajectories of error signals without control (left) and with impulsive control (right).

5.2. Image cryptosystem based on bit-level permutation and drive-response signals

The image cryptosystem is built with the help of methodologies proposed in [4, 45, 48], as shown in Figure 4(left). The cryptosystem consists of transmitter end and receiver end where the drive-response signals are generated. Then the signals are delivered into the encryption box and decryption box to cipher the plain image and decrypt the ciphered image. The encryption scheme includes bit-level permutation (confusion) and pixel-level diffusion based on the drive signal. The full details are given as follows.

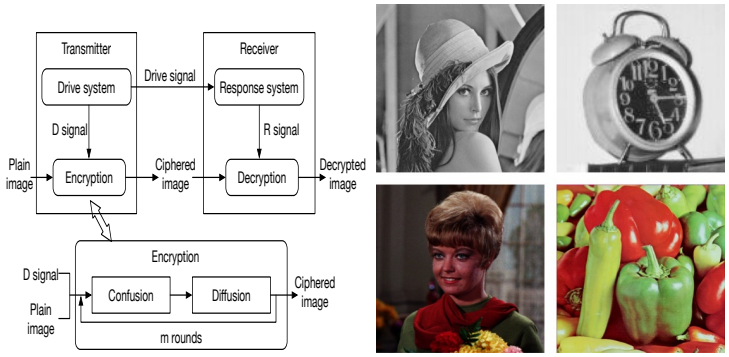

Figure 4: Flow chart (left) and test images (right) of the image cryptosystem.

(1) Bit-level permutation. First, the plain image (M×N) is divided into 8 binary images. Then, 1-8 bit binary images are combined into a whole image (M×8N) which is permuted by the Arnold cat map. The Arnold cat map is defined by

$$\begin{bmatrix} x' \\ y' \end{bmatrix} = \begin{bmatrix} 1 & p \\ q & pq+1 \end{bmatrix} \begin{bmatrix} x \\ y \end{bmatrix} \bmod \begin{bmatrix} M \\ 8N \end{bmatrix}, \tag{30}$$

where (x, y) represents the coordinate in the bit-level combined image and (x', y') represents the new coordinate. The parameters p and q are determined by

$$p = (|s[8xN + y + 10^3] \times 10^5|) \text{mod} M, \; q = (|s[\text{end} - 8xN - y] \times 10^5|) \text{mod} N,$$

where s is the combination of drive signals s_1 and s_2. Through the bit-level permutation, the pixels' values and positions are changed and the bits in all the bit plane are changed, which is different from Zhu's algorithm [48].

(2) Pixel-level diffusion. For the pixel-level diffusion, we apply the drive signal to the diffusion phase proposed in [48] instead of the chaotic sequence generated by the logistic map. The main procedures are sketched as follows:

Step 1: the pixels in the permuted image are scanned from upper-left to lower-right and form a permuted sequence.

Step 2: each pixel is diffused by $c[i+1] = p[i+1] \oplus \{\{[4 \times (c[i]/1000) \times (1 - c[i]/1000) \times 1000] + (s[i+100] \times 10^5) \text{mod} 256\} \text{mod} 256\}$, where c, p and s represent the ciphered sequence, permuted sequence and drive signal, respectively.

Step 3: the ciphered sequence is reshaped to be the ciphered image.

5.3. Experimental results

This subsection reports the performance analysis for the image cryptosystem. Four different images, including Lena (gray 512×512), Clock (gray 128×128), Lady (color 256×256), and Pepper (color 512×512) as shown in Figure 4(right), are tested to show the effectiveness. For color images, the red, green and blue components are extracted to be ciphered or decrypted, respectively. Figure 5 illustrates the plain images, ciphered images, decrypted images of Lena and Lady. Visually, the ciphered images are quite different from the plain images whereas the decrypted images are identical with the plain images. A good cryptosystem should resist various attacks, so the key space

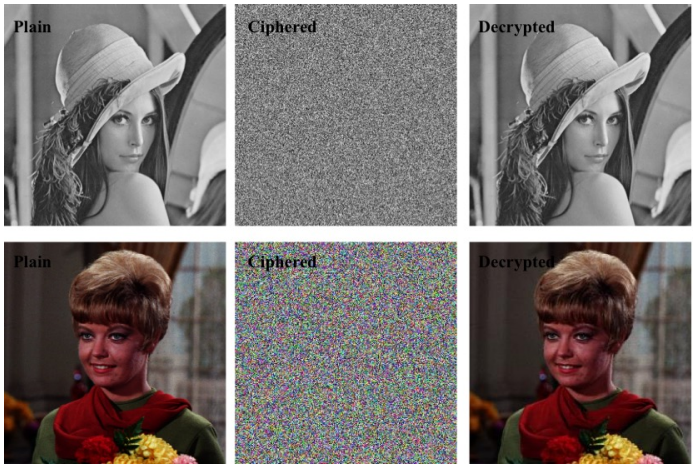

Figure 5: Lena image (top) and Lady image (bottom).

analysis, differential analysis and statistical analysis are performed to demonstrate the security as follows.

(1) Key space analysis. The encryption scheme includes the following keys: the parameters of the spatiotemporal chaotic neural networks, the synchronous time, and the initial condition of the ciphered sequence. As stated in [4, 48], the key space is large enough in theory to resist the brute-force attack and the encryption scheme is sensitive to the secret keys. Moreover, the stochastic factor (Brownian motion) can also be treated as the key, since the used drive-response system is stochastic chaotic system. The irreproducibility of stochastic factor improves the security of the scheme.

Table 1: NPCR and UACI performance compared with LM, Refs. [48] and [17].

	Round	Proposed scheme	LM	Ref. [48]	Ref [17]
NPCR	1	0.0059	0.0043	0.004223	0.0003357
	2	0.8964	0.8643	0.8120	0.03328
	3	0.9964	0.9958	0.9961	0.7993
UACI	1	0.019	0.0014	0.001366	0.00008774
	2	0.3016	0.2904	0.2739	0.00008774
	3	0.3347	0.3350	0.3340	0.2186

(2) Differential analysis. A good encryption scheme should be sensitive to the plain images because an adversary may find out the relationship between the ciphered images and the plain images through observing the change of the ciphered results caused by slight change of the plain images. Generally, the number of pixels change rate (NPCR) and unified average changing intensity (UACI) are employed to test the sensitivity. The NPCR and UACI are calculated by

$$\text{NPCR} = \frac{\Sigma_{i,j} D(i,j)}{M \times N} \times 100\%, \ \text{UACI} = \frac{\Sigma_{i,j} |c_1(i,j) - c_2(i,j)|}{255 \times M \times N} \times 100\%, \quad (31)$$

where c_1 and c_2 are two ciphered images and $D(i,j)$ is defined by

$$D(i,j) = \begin{cases} 1, & c_1(i,j) \neq c_2(i,j), \\ 0, & \text{otherwise.} \end{cases}$$

Here, we use two plain images: original Lena image and the other Lena image obtained by changing 1 bit of (511,511). Then, these two images are ciphered by the same keys to calculate NPCR and UACI. The results are listed in Table 1 compared with Refs. [48] and [17]. To testify the effect of drive-response signals, we also perform the proposed encryption process based on the logistic map (LM) instead of drive-response signals. By comparison in Table 1, both NPCR and UACI reach higher performance than LM and Refs. [17, 48]. Therefore, the proposed algorithm is more efficient to resist differential attack.

(3) Statistical analysis. To demonstrate the robustness of cryptosystem, we also perform analysis of histogram, entropy, and correlation of the plain images and ciphered images. The ciphered images should process certain random properties, which

means the decrease in variance of histogram, closeness of entropy to 8, and small correlation of plain images and ciphered images and of two adjacent pixels in ciphered images. Figure 6 illustrates the histograms of the plain Lena image, ciphered image, and decrypted image. Figure 7 depicts the correlation distribution of two adjacent pixels in horizontal, vertical, and diagonal directions. The significant reduction in correlation indicates that the correlation of adjacent pixels in the plain images has been removed. The quantification of the ciphered results is presented in Tables 2-4, including variance of histogram [45], entropy, and correlation of the plain images and ciphered images (CPC), and correlations of two adjacent pixels. The correlations of two adjacent pixels of color images are absolute averages of RGB components. From

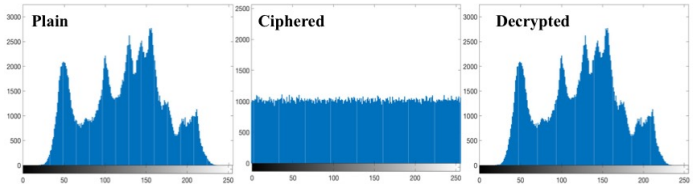

Figure 6: Histograms of Lena images.

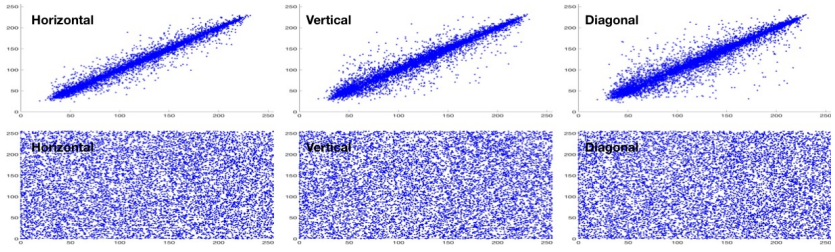

Figure 7: Correlation of adjacent pixels in plain image (top) and ciphered image (bottom).

Table 2: Variance of histogram.

Image	Lena	Clock	Lady	Pepper
Original	6.37e5	2.40e4	9.09e5	3.31e6
Ciphered	1.04e3	56.02	876.63	3.41e3
Decrypted	6.37e5	2.40e4	9.09e5	3.31e6

Table 3: Entropy and CPC of different images.

Image	Lena	Clock	Lady	Pepper
Entropy	7.9993	7.9901	7.9971	7.9993
CPC	2.24e-4	0.015	-5.27e-3	1.20e-3

Figure 6 and Table 2, the variances of histograms of ciphered images significantly decrease compared with those of plain images. The uniformity of the histograms of the ciphered images makes statistic attacks difficult. As a result, the proposed method is able to resist chosen-plaintext or known-plaintext attacks. From Tables 3 and 4, the entropy 7.9993 of Lena is close to 8 and the correlations of two adjacent pixels agree with the description of Figure 7, which also imply the random-like appearance of the ciphered images.

Table 4: Correlations of two adjacent pixels in horizontal, vertical, and diagonal directions.

Image		Horizontal	Vertical	Diagonal	Average
Lena	Original	0.9726	0.9863	0.9596	0.9728
	Ciphered	-0.0018	-0.0018	-0.0018	0.0018
Clock	Original	0.9445	0.9518	0.9518	0.9494
	Ciphered	0.0025	0.0079	0.0131	7.833e-3
Lady	Original	0.9677	0.9596	0.9453	0.9575
	Ciphered	4.17e-3	0.0056	3.28e-3	4.35e-3
Pepper	Original	0.9802	0.9814	0.9641	0.9753
	Ciphered	1.03e-3	8.64e-4	7.97e-4	8.98e-4

Remark 7. In comparison with recent image encryption application of neural networks [4, 27, 37], the proposed scheme is more robust to statistic attacks because the absolute average correlation of two adjacent pixels for Lady and Pepper is 2.63e-3 which is smaller than 3.35e-3 of [37] and 3.40e-3 of [27] and the correlation for Lena is smaller than 9.20e-3 of [4]. Besides, the proposed scheme is robust to differential attack because NPCR reaches 0.99 and UACI reaches 0.33.

6. Conclusion

In this paper, we establish sufficient conditions for global exponential stability of SIRDNNs based an impulsive inequality involving infinite delay. The asymptotic behaviour of SIRDNNs with S-type distributed delays is studied by truncating the infinite delay to finite delay and an infinitesimal and the global exponential stability is established by the Lyaponov method. Finally, the applicability of the proposed theories is verified by some illustrative examples and the application to image encryption. Future work will focus on SIRDNNs with S-type distributed delays and large impulse. To achieve the stability, stronger conditions on the S-type distributed delays are needed. Besides, the dissipativity theory provides primary structure for synthesis and analysis in several domains of control engineering problems [19, 20, 21], so another future work will concentrate on the dissipativity state estimation for SIRDNNs.

Acknowledgment

This work was supported by the National Key Research and Development Program of China (2018YFD0901601), National Natural Science Foundation of China (11771014, 91430106, 31772844), Fundamental Research Funds for the Central Universities (No. 06500073), the Major Basic Research Projects of Shandong Natural Science Foundation (2018A07), and China Scholarship Council (File No. 201706330011).

Appendix A. Proof of Lemma 3

Proof. First, we prove that $\nu(t) \leq \mu(t)$ for $t \in [t_0, t_1)$. If it is not true, there exists $t^* \in [t_0, t_1)$ such that $\nu(t^*) > \mu(t^*)$, indicating that there exists $\bar{t} \in [t_0, t^*)$ satisfying

$$\nu(\bar{t}) = \mu(\bar{t}),\ D^+\nu(\bar{t}) \geq D^+\mu(\bar{t}),\ \nu(t) \leq \mu(t), \tag{32}$$

where $t \in [t_0, \bar{t})$, furthermore, $\bar{\nu}(\bar{t}) \leq \bar{\mu}(\bar{t})$. From the condition of the Lemma, we see

$$D^+\nu(\bar{t}) \leq \Phi(\bar{t}, \nu(\bar{t}), \bar{\nu}(\bar{t})) \leq \Phi(\bar{t}, \mu(\bar{t}), \bar{\mu}(\bar{t})) < D^+\mu(\bar{t}), \tag{33}$$

which contradicts (32). Hence, $\nu(t) \leq \mu(t)$ for $t \in [t_0, t_1)$. Then, when $t = t_1$, the monotonicity of I_k implies that $\nu(t_1) \leq I_k(\nu(t_1^-)) \leq I_k(\mu(t_1^-)) \leq \mu(t_1)$. Based on the mathematical induction, the lemma is proved by using the similar process. □

Appendix B. Proof of Lemma 4

Proof. Since $a+\frac{b}{\gamma}>0$ and $a+\frac{b}{\gamma}+\frac{\ln\gamma}{\rho}<0$, there exists a positive constant $\lambda'<-\frac{\ln\gamma}{\rho}$ such that $-\lambda'+a+\frac{b}{\gamma}e^{-(\lambda'+\frac{\ln\gamma}{\rho})\tau}<0$. Let $\Phi(t,x,y)=ax+by+o(\epsilon)$,

$$\mu(t)=\begin{cases}\|\phi\|_{PC^b}, & t\le t_0,\\ \gamma^{k-1}M'e^{\lambda'(t-t_0)}-\frac{o(\epsilon)}{a+b}, & t\in[t_{k-1},t_k),\end{cases}$$

where $M'=\|\phi\|_{PC^b}+\frac{o(\epsilon)}{a+b}$. Obviously, when $t\le t_0$, $\nu(t)\le\mu(t)$. For $t\in(t_{k-1},t_k)$, we have

$$\begin{aligned}
D^+\nu(t)&\le a\nu(t)+b\sup_{-\tau\le\theta\le0}\nu(t+\theta)+o(\epsilon)=\Phi(t,\nu(t),\bar\nu(t)),\\
D^+\mu(t)&=\gamma^{k-1}\lambda'M'e^{\lambda'(t-t_0)}>\gamma^{k-1}(a+\frac{b}{\gamma}e^{-(\lambda'+\frac{\ln\gamma}{\rho})\tau})M'e^{\lambda'(t-t_0)}\\
&\ge a\mu(t)+bM'\gamma^{k-1}\sup_{-\tau\le\theta\le0}\gamma^{\frac{\theta}{\rho}-1}e^{\lambda'(t+\theta-t_0)}+\frac{ao(\epsilon)}{a+b}\\
&\ge a\mu(t)+b\sup_{-\tau\le\theta\le0}\mu(t+\theta)+o(\epsilon)=\Phi(t,\mu(t),\bar\mu(t)).
\end{aligned}\tag{34}$$

From Lemma 3, we know that

$$\nu(t)\le\gamma^{k-1}M'e^{\lambda'(t-t_0)}-\frac{o(\epsilon)}{a+b}\le\frac{1}{\gamma}M'e^{-\lambda(t-t_0)}-\frac{o(\epsilon)}{a+b},$$

where $\lambda=-(\lambda'+\frac{\ln\gamma}{\rho})>0$. As $\epsilon\to0$, we obtain that $\Phi(t)\le Me^{-\lambda(t-t_0)}\|\phi\|_{PC^b}$ for $t\in[t_0,+\infty)$ where $M=1/\gamma$. □

Appendix C. Proof of Lemma 6

Proof. Combining Lemma 5 with 4, we simply need to prove the result for $a+\frac{b}{\gamma}=0$. The details of the proof are similar to those of Lemma 4, so we give an outline focusing on the different parts. Since $\frac{\ln\gamma}{\rho}<0$, there exists a positive constant $\lambda'<-\frac{\ln\gamma}{\rho}$ such that $-\lambda'+a+\frac{b}{\gamma}e^{-(\lambda'+\frac{\ln\gamma}{\rho})\tau}<0$. Let $\mu(t)=\gamma^{k-1}M''e^{\lambda'(t-t_0)}$ for $t\in[t_{k-1},t_k)$, $k\in\mathbb{N}^+$, where $M''=\|\phi\|_{PC^b}$. For $t\in(t_{k-1},t_k)$, if ϵ is small enough, we have

$$\begin{aligned}
D^+\mu(t)&=\gamma^{k-1}\lambda'M''e^{\lambda'(t-t_0)}>(a+\frac{b}{\gamma}e^{-(\lambda'+\frac{\ln\gamma}{\rho})\tau})\gamma^{k-1}M''e^{\lambda'(t-t_0)}+o(\epsilon)\\
&\ge a\mu(t)+b\sup_{-\tau\le\theta\le0}\mu(t+\theta)+o(\epsilon)=\Phi(t,\mu(t),\bar\mu(t)).
\end{aligned}\tag{35}$$

As proof of Lemma 4, we conclude that there exist positive constants M and λ such that $\nu(t) \leq Me^{-\lambda(t-t_0)}\|\phi\|_{PC^b}$ for $t \in [t_0, +\infty)$ where $\lambda = -(\lambda' + \frac{\ln\gamma}{\rho}) > 0$ and $M = 1/\gamma$. Then, the Lemma is proved. □

Appendix D. Proof of Lemma 7

Proof. Denote $\lambda = a + \frac{\ln\gamma}{\rho}$. Since $a + b\gamma + \frac{\ln\gamma}{\rho} < 0$, then $-\frac{b\gamma}{\lambda} < 1$, indicating that there exists a constant $n \in (0, 1)$ such that $-\frac{b\gamma}{\lambda} < n$. From Lemma 3, we derive the following comparison system

$$\begin{cases} \dfrac{d\mu(t)}{dt} = a\mu(t) + b \sup\limits_{-\tau\leq\theta\leq 0} \mu(t+\theta) + o(\epsilon) + \epsilon', t \neq t_k, t \geq t_0, \\ \mu(t_k) = \gamma\mu(t_k^-),\ k \in \mathbb{N}^+, \\ \mu(t) = \|\phi\|_{PC^b},\ t \leq t_0, \end{cases} \tag{36}$$

for any $\epsilon' > 0$. Obviously, $\nu(t) \leq \mu(t)$ for $t \in [t_0, +\infty)$. Then we shall prove that $\mu(t)$ is bounded. Using similar process of Lemma 5 in [37], we know that $\mu(t) \leq \mu(t_{k-1})$ for $t \in [t_{k-1}, t_k)$. If $\mu(t)$ is not bounded, there exists $k^* \in \mathbb{N}^+$ such that $\mu(t_{k^*}) = M$ and $\mu(t) < M$ for $t_0 \leq t < t_{k^*}$ where $M > \frac{4\gamma}{1-n}\max\{\|\phi\|_{PC^b}, -\frac{o(\epsilon)+\epsilon'}{\lambda}\}$. By the formula for the variation of parameters and Lemma 3.1 in [41], we see that

$$\begin{aligned} \mu(t_{k^*}) &\leq \gamma e^{\lambda(t_{k^*}-t_0)}\mu(t_0) + (o(\epsilon)+\epsilon')\gamma\int_{t_0}^{t_{k^*}} e^{\lambda(t_{k^*}-s)}ds \\ &\quad + b\gamma\int_{t_0}^{t_{k^*}} e^{\lambda(t_{k^*}-s)} \sup_{-\tau\leq\theta\leq 0}\mu(s+\theta)ds \\ &\leq \gamma\|\phi\|_{PC^b} - \frac{o(\epsilon)+\epsilon'}{\lambda}\gamma(1-e^{\lambda(t_{k^*}-t_0)}) - \frac{b\gamma M}{\lambda}(1-e^{\lambda(t_{k^*}-t_0)}) \\ &\leq \frac{1-n}{2}M + nM < M. \end{aligned} \tag{37}$$

This is contradiction. Hence, $\mu(t)$ and $\nu(t)$ are bounded. □

Appendix E. Proof of Lemma 8

Proof. From Lemma 3, we derive the following comparison system

$$\begin{cases} \dfrac{d\tilde{\mu}(t)}{dt} = a\tilde{\mu}(t) + b\tilde{\mu}(t-\tau) + \epsilon', t \neq t_k, t \geq t_0, \\ \tilde{\mu}(t_k) = \gamma\tilde{\mu}(t_k^-),\ k \in \mathbb{N}^+, \\ \tilde{\mu}(t) = \|\tilde{\phi}\|_{PC^b},\ t \leq t_0, \end{cases} \tag{38}$$

for any $\epsilon' > 0$. Obviously, $\tilde{\nu}(t) \leq \tilde{\mu}(t)$ for $t \in [t_0, +\infty)$. First, let us consider the function $\delta(\lambda) = \lambda + a + b\gamma e^{\lambda\tau} + \frac{\ln\gamma}{\rho}$, where $\lambda \in [0, +\infty)$. Since $a + b\gamma + \frac{\ln\gamma}{\rho} < 0$ and $b \geq 0$, we obtain $\delta(0) < 0$ and $\delta(\lambda)$ is continuous and monotonous, furthermore, $\delta(\lambda) \to +\infty$ as $\lambda \to +\infty$. Consequently, there exists a constant $\lambda' > 0$ such that $\delta(\lambda') < 0$. Then we shall prove that $\tilde{\mu}(t) \leq M''e^{-\lambda'(t-t_0)} + k\epsilon'$ where $t \geq t_0$, $M'' = \gamma\|\tilde{\phi}\|_{PC^b([-\tau,t_0],\mathbb{R}^+)}$, and $k = -\frac{\gamma}{a+b\gamma+\frac{\ln\gamma}{\rho}}$. If it is not true, there exists $t^* > t_0$ such that $\tilde{\mu}(t^*) \geq M''e^{-\lambda'(t^*-t_0)} + k\epsilon'$ and $\tilde{\mu}(t) < M''e^{-\lambda'(t-t_0)} + k\epsilon'$ for $t_0 \leq t < t^*$. By the formula for the variation of parameters and Lemma 3.1 in [41], we see that

$$\begin{aligned} \tilde{\mu}(t^*) \leq\ & \gamma e^{\alpha(t^*-t_0)}\phi(t_0) + \epsilon'\gamma\int_{t_0}^{t^*} e^{\alpha(t^*-s)}ds + b\gamma\int_{t_0}^{t^*} e^{\alpha(t^*-s)}\tilde{\mu}(s-\tau)ds \\ \leq\ & M''e^{\alpha(t^*-t_0)} + (bk+1)\gamma\epsilon'\int_{t_0}^{t^*} e^{\alpha(t^*-s)}ds + M''e^{\alpha t^* + \lambda' t_0}b\gamma e^{\lambda'\tau}\int_{t_0}^{t^*} e^{-(\alpha+\lambda')s}ds \\ <\ & M''e^{\alpha(t^*-t_0)} + k\epsilon'(1 - e^{\alpha(t^*-t_0)}) - M''e^{\alpha t^* + \lambda' t_0}(\alpha+\lambda')\int_{t_0}^{t^*} e^{-(\alpha+\lambda')s}ds \\ \leq\ & M''e^{\alpha(t^*-t_0)} + k\epsilon' + M''e^{-\lambda'(t^*-t_0)} - M''e^{\alpha(t^*-t_0)} \\ =\ & k\epsilon' + M''e^{-\lambda'(t^*-t_0)}, \end{aligned}$$

where $\alpha = a + \frac{\ln\gamma}{\rho}$. This is contradiction. Hence, $\tilde{\mu}(t) \leq \tilde{\nu}(t) \leq M''e^{-\lambda'(t-t_0)} + k\epsilon'$ for $t \in [t_0, +\infty)$, furthermore, the lemma is proved as $\epsilon' \to 0$. □

References

[1] Ali, M. S., Saravanakumar, R., Ahn, C. K., & Karimi, H. R. (2017). Stochastic H_∞ filtering for neural networks with leakage delay and mixed time-varying delays. *Information Sciences*, *388-389*, 118–134.

[2] Arik, S. (2016). Dynamical analysis of uncertain neural networks with multiple time delays. *International Journal of Systems Science*, *47*, 730–739.

[3] Bao, H., Park, J. H., & Cao, J. (2016). Exponential synchronization of coupled stochastic memristor-based neural networks with time-varying probabilistic delay coupling and impulsive delay. *IEEE Transactions on Neural Networks and Learning Systems*, *27*, 190–201.

[4] Chen, W.-H., Luo, S., & Zheng, W. X. (2016). Impulsive synchronization of reaction-diffusion neural networks with mixed delays and its application to image encryption. *IEEE Transactions on Neural Networks and Learning Systems*, *27*, 2696–2710.

[5] Esteves, S., Gökmen, E., & Oliveira, J. J. (2013). Global exponential stability of nonautonomous neural network models with continuous distributed delays. *Applied Mathematics and Computation*, *219*, 9296–9307.

[6] Fridrich, J. (1998). Symmetric ciphers based on two-dimensional chaotic maps. *International Journal of Bifurcation and Chaos*, *8*, 1259–1284.

[7] Gawarecki, L., & Mandrekar, V. (2011). *Stochastic Differential Equations in Infinite Dimensions: with Applications to Stochastic Partial Differential Equations*. Springer Berlin Heidelberg.

[8] Halanay, A. (1966). *Differential Equations: Stability, Oscillations, Time Lags*. New York: Academic press.

[9] Hattne, J., Fange, D., & Elf, J. (2005). Stochastic reaction-diffusion simulation with MesoRD. *Bioinformatics*, *21*, 2923–2924.

[10] He, W., Qian, F., & Cao, J. (2017). Pinning-controlled synchronization of delayed neural networks with distributed-delay coupling via impulsive control. *Neural Networks*, *85*, 1–9.

[11] He, X., Yu, J., Huang, T., Li, C., & Li, C. (2018). Average quasi-consensus algorithm for distributed constrained optimization: impulsive communication framework. *IEEE Transactions on Cybernetics*, *Early Access*, 1–10.

[12] Huang, T., Li, C., Duan, S., & Starzyk, J. A. (2012). Robust exponential stability of uncertain delayed neural networks with stochastic perturbation and impulse effects. *IEEE Transactions on Neural Networks and Learning Systems*, *23*, 866–875.

[13] Jiang, M., Mu, J., & Huang, D. (2016). Globally exponential stability and dissipativity for nonautonomous neural networks with mixed time-varying delays. *Neurocomputing*, *205*, 421–429.

[14] Lakshmanan, S., Prakash, M., Lim, C. P., Rakkiyappan, R., Balasubramaniam, P., & Nahavandi, S. (2018). Synchronization of an inertial neural network with time-varying delays and its application to secure communication. *IEEE Transactions on Neural Networks and Learning Systems*, *29*, 195–207.

[15] Li, X., & Bohner, M. (2012). An impulsive delay differential inequality and applications. *Computers & Mathematics with Applications*, *64*, 1875–1881.

[16] Li, X., & Cao, J. (2017). An impulsive delay inequality involving unbounded time-varying delay and applications. *IEEE Transactions on Automatic Control*, *62*, 3618–3625.

[17] Lian, S., Sun, J., & Wang, Z. (2005). A block cipher based on a suitable use of the chaotic standard map. *Chaos, Solitons & Fractals*, *26*, 117–129.

[18] Liu, K. (2005). *Stability of Infinite Dimensional Stochastic Differential Equations with Applications*. Chapman and Hall/CRC.

[19] Manivannan, R., Panda, S., Chong, K. T., & Cao, J. (2018). An Arcak-type state estimation design for time-delayed static neural networks with leakage term based on unified criteria. *Neural Networks*, *106*, 110–126.

[20] Manivannan, R., Samidurai, R., Cao, J., Alsaedi, A., & Alsaadi, F. E. (2017). Global exponential stability and dissipativity of generalized neural networks with time-varying delay signals. *Neural Networks*, *87*, 149–159.

[21] Manivannan, R., Samidurai, R., Cao, J., Alsaedi, A., & Alsaadi, F. E. (2018). Design of extended dissipativity state estimation for generalized neural networks with mixed time-varying delay signals. *Information Sciences*, *424*, 175–203.

[22] Oliveira, J. J. (2017). Global exponential stability of nonautonomous neural network models with unbounded delays. *Neural Networks*, *96*, 71–79.

[23] Qi, J., Li, C., & Huang, T. (2014). Stability of delayed memristive neural networks with time-varying impulses. *Cognitive Neurodynamics*, *8*, 429–436.

[24] Rakkiyappan, R., Dharani, S., & Zhu, Q. (2015). Synchronization of reaction-diffusion neural networks with time-varying delays via stochastic sampled-data controller. *Nonlinear Dynamics*, *79*, 485–500.

[25] Saravanakumar, R., Ali, M. S., & Karimi, H. R. (2017). Robust H_∞ control of uncertain stochastic Markovian jump systems with mixed time-varying delays. *International Journal of Systems Science*, *48*, 862–872.

[26] Selvaraj, P., Sakthivel, R., & Kwon, O. M. (2018). Finite-time synchronization of stochastic coupled neural networks subject to Markovian switching and input saturation. *Neural Networks*, *105*, 154–165.

[27] Shanmugam, L., Mani, P., Rajan, R., & Joo, Y. H. (2018). Adaptive synchronization of reaction-diffusion neural networks and its application to secure communication. *IEEE Transactions on Cybernetics*, *Early Access*, 1–12.

[28] Sheng, Y., & Zeng, Z. (2018). Impulsive synchronization of stochastic reaction-diffusion neural networks with mixed time delays. *Neural Networks*, *103*, 83–93.

[29] Sheng, Y., Zhang, H., & Zeng, Z. (2017). Synchronization of reaction-diffusion neural networks with Dirichlet boundary conditions and infinite delays. *IEEE Transactions on Cybernetics*, *47*, 3005–3017.

[30] Temam, R. (2012). *Infinite-Dimensional Dynamical Systems in Mechanics and Physics*. Springer Science & Business Media.

[31] Wang, L. (2008). *Delayed Recurrent Neural Networks*. Beijing, China: Science Press.

[32] Wang, X., Li, C., Huang, T., & Chen, L. (2014). Impulsive exponential synchronization of randomly coupled neural networks with Markovian jumping and mixed model-dependent time delays. *Neural Networks*, *60*, 25–32.

[33] Wang, Z., Liu, Y., Yu, L., & Liu, X. (2006). Exponential stability of delayed recurrent neural networks with Markovian jumping parameters. *Physics Letters A*, *356*, 346–352.

[34] Wei, T., Lin, P., Zhu, Q., Wang, L., & Wang, Y. (2018). Dynamical behavior of nonautonomous stochastic reaction-diffusion neural-network models. *IEEE Transactions on Neural Networks and Learning Systems*, *Early Access*, 1–6.

[35] Wei, T., Wang, L., & Wang, Y. (2017). Existence, uniqueness and stability of mild solutions to stochastic reaction-diffusion Cohen-Grossberg neural networks with delays and Wiener processes. *Neurocomputing*, *239*, 19–27.

[36] Wei, T., Wang, Y., & Wang, L. (2018). Robust exponential synchronization for stochastic delayed neural networks with reaction-diffusion terms and Markovian jumping parameters. *Neural Processing Letters*, *48*, 979–994.

[37] Wei, T., Yao, Q., Lin, P., & Wang, L. (2018). Adaptive synchronization of stochastic complex dynamical networks and its application. *Neural Computing and Applications*, *Online*, 1–14.

[38] Xu, D., Li, B., Long, S., & Teng, L. (2014). Moment estimate and existence for solutions of stochastic functional differential equations. *Nonlinear Analysis: Theory, Methods & Applications*, *108*, 128–143.

[39] Xu, L., & Ge, S. S. (2018). Asymptotic behavior analysis of complex-valued impulsive differential systems with time-varying delays. *Nonlinear Analysis: Hybrid Systems*, *27*, 13–28.

[40] Yang, X., Cao, J., & Yang, Z. (2013). Synchronization of coupled reaction-diffusion neural networks with time-varying delays via pinning-impulsive controller. *SIAM Journal on Control and Optimization*, *51*, 3486–3510.

[41] Yang, Z., & Xu, D. (2007). Robust stability of uncertain impulsive control systems with time-varying delay. *Computers & Mathematics with Applications*, *53*, 760–769.

[42] Yang, Z., & Xu, D. (2007). Stability analysis and design of impulsive control systems with time delay. *IEEE Transactions on Automatic Control*, *52*, 1448–1454.

[43] Zhang, Q., Wei, X., & Xu, J. (2009). Global exponential stability for nonautonomous cellular neural networks with unbounded delays. *Chaos, Solitons & Fractals*, *39*, 1144–1151.

[44] Zhang, W., Huang, T., He, X., & Li, C. (2017). Global exponential stability of inertial memristor-based neural networks with time-varying delays and impulses. *Neural Networks*, *95*, 102–109.

[45] Zhang, Y.-Q., & Wang, X.-Y. (2014). A symmetric image encryption algorithm based on mixed linear–nonlinear coupled map lattice. *Information Sciences*, *273*, 329–351.

[46] Zhu, Q., & Cao, J. (2012). Stability analysis of Markovian jump stochastic BAM neural networks with impulse control and mixed time delays. *IEEE Transactions on Neural Networks and Learning Systems*, *23*, 467–479.

[47] Zhu, Q., Cao, J., & Rakkiyappan, R. (2015). Exponential input-to-state stability of stochastic Cohen-Grossberg neural networks with mixed delays. *Nonlinear Dynamics*, *79*, 1085–1098.

[48] Zhu, Z.-L., Zhang, W., Wong, K.-W., & Yu, H. (2011). A chaos-based symmetric image encryption scheme using a bit-level permutation. *Information Sciences*, *181*, 1171–1186.